Optical second-order skyrmionic hopfion

Ehrmanntraut, Daniel; Droop, Ramon; Sugic, Danica; Otte, Eileen; Dennis, Mark R.; Denz, Cornelia

DOI:
10.1364/OPTICA.487989

Research Article Vol. 10, No. 6 / June 2023 / Optica 725

OPTICA

Optical second-order skyrmionic hopfion

Daniel Ehrmanntraut,[1,*] Ramon Droop,[1] Danica Sugic,[2,3] Eileen Otte,[1,4,5] Mark R. Dennis,[2,3,6] and Cornelia Denz[1,7]

[1]Institute of Applied Physics, University of Münster, Corrensstr. 2/4, 48149 Münster, Germany
[2]School of Physics and Astronomy, University of Birmingham, Birmingham B15 2TT, UK
[3]H H Wills Physics Laboratory, University of Bristol, Bristol BS8 1TL, UK
[4]Geballe Laboratory for Advanced Materials, Stanford University, 476 Loomita Mall, Stanford, California 94305, USA
[5]Center for Soft Nanoscience, University of Münster, Busso-Peus-Str. 10, 48149 Münster, Germany
[6]EPSRC Centre for Doctoral Training in Topological Design, University of Birmingham, Birmingham B15 2TT, UK
[7]Physikalisch-Technische Bundesanstalt, Bundesallee 100, 38116 Braunschweig, Germany
*d.ehrmanntraut@uni-muenster.de

Received 15 February 2023; revised 23 April 2023; accepted 10 May 2023; published 8 June 2023

Due to their topological stability and spatial confinement, particle-like field configurations have gained significant interest in many areas of physics. Only recently, the first skyrmionic hopfion was proposed in light, but its higher-order analog in optics has stayed a theoretical construct so far, and direct experimental observations also prove difficult in non-optical systems. Here we overcome this challenge by the experimental realization and analysis of a second-order skyrmionic hopfion in the polarization and phase texture of a paraxial light field in three-dimensional space. Thereby, we exemplify advanced control of observed parameters in a localized space, pioneering further experimental studies on higher-order hopfions in optics and beyond.

https://doi.org/10.1364/OPTICA.487989

1. INTRODUCTION

The spatial customization of light in its different degrees of freedom, such as amplitude, phase, and/or polarization, has proven to be an impactful tool in various research areas (see [1–3] and references therein): it enables complex optical micro- and nano-manipulation, advances material machining down to the nanoscale, facilitates novel approaches for classical as well as quantum communication, or can serve as a model to study scientific problems in non-optical systems [4–7]. In recent years, the overlap of this field of research, i.e., structured light, with the area of topology, has attracted increasing interest due to the huge potential of implementing topologically protected, stable spatial constructs of light in the above named applications.

In this context, singular optics gives special attention to points and lines of undefined phase (phase singularities) in phase vortex structures or of undefined properties of polarization states, namely, polarization singularities in spatial polarization structures [8–10]. These singularities are of topological nature themselves while building the "skeleton" of the structured light field surrounding it in three-dimensional (3D) space. Besides being of fundamental interest, these singular light fields with integer singularity indices have found different applications, e.g., as information carriers in optical communication [11]. Also, it has been shown that these singularities in phase and polarization [12–14] as well as other 1D optical structures such as light filaments [15] can actually be plaited into mathematical knots. Such findings have opened the door to studying complex topological constructs in light, whereby, recently, even particle-like 2D and 3D topologies such as optical skyrmions and (skyrmionic) hopfions have become accessible. The investigation of these optical constructs is still in its infancy with its best future applications still to be identified.

Skyrmions originate from a potential description for atomic nuclei [16,17], representing a field configuration that can arise in 2D ("baby skyrmion") or even 3D systems [18]. They are topological maps from n-dimensional (nD) space to the nD sphere. They currently are of high interest in, e.g., condensed matter physics, where 2D magnetic skyrmions are proposed for efficient non-volatile memory units [19,20] due to the stability provided by the topological structure. In analogy to the spin structure of these magnetic skyrmions, similar 2D structures in light fields—optical baby skyrmions—have been realized [21–25]. These structures are generally characterized by an integer invariant; if a baby skyrmion carries an invariant with its absolute >1, it is referred to be of "higher order." These higher-order baby skyrmions have been proposed in both magnetic [26–29] and optical systems [24,25,30]. To facilitate full 3D skyrmions, one needs to achieve a mapping from a 4D sphere to 3D space. This can be done by choosing a special parametrization of the 4D sphere, the hopf fibration, which is defined by a map from the 4D sphere to a 3D sphere. Projections of this parametrization into 3D space are called hopfions, which are self-contained, localized structures in real space and therefore particle-like in nature, just like skyrmions.

Hopfions have been theoretically predicted and experimentally verified in various systems, including high-energy physics [31–33], electro (-magnetic) field lines [34–38] with an interesting analogy between electromagnetic and gravitational hopfions [39], liquid crystals [40], a fluid of magnetic nanoplates [41], atom layers [42], and the polarization [43] or the polarization as well as phase texture of structured light [44]. If all four parameters of the 4D sphere have a physical meaning in 3D space, the hopfion is actually the projection of the entire 4D sphere, making it also a 3D skyrmion and thus the name "skyrmionic hopfion." Therefore, it combines two topological aspects, namely, the properties of a 3D skyrmion as well as a hopfion. Similar to baby skyrmions, one can define a topological invariant for the skyrmionic hopfion and could construct higher-order versions of it. In the case of the optical skyrmionic hopfion, this parametrization is the combination of phase and the three Stokes parameters $S_{1,2,3}$ that span the Poincaré sphere and characterize the polarization of the light field [44].

Up to now, research has mainly focused on 2D skyrmion configurations and theoretical descriptions of hopfions—in optics as well as in other fields of physics. Especially the experimental generation and analysis of 3D topological structures remains a challenge in many research fields. In this work, we extend rarely existing experimental realizations of these topological structures by providing the first experimental realization and analysis of a higher-order skyrmionic hopfion in structured light. We exemplify these higher-order constructs by presenting a second-order skyrmionic hopfion formed by the polarization and phase texture in a paraxial field in 3D space. For this purpose, in the following, we first give a brief overview on higher-order skyrmionic hopfions and how to embed them in light (Section 2). Subsequently, we present the successful experimental realization in the form of polarization fibration in 3D space and the respective skyrme number (Section 3); our results are discussed in Section 4. The presented results open the door to further experimental investigation of different higher-order integer invariants of confined particle-like light fields and thereby unlock the potential of these fields for future applications such as data storage and communication based on topological invariants.

2. HIGHER ORDERS OF THE SKYRMIONIC HOPFION

A skyrmionic hopfion can be regarded in its two natures: a skyrmionic nature, arising from covering of a unit-sphere in 4D space (denoted three-sphere $\mathbb{S}^3$), and its hopf nature, stemming from linking of the projected fibers. Associated with each topological aspect is an integer quantity: the skyrme number, counting the extent of covering the three-sphere, and the hopf invariant, giving the linking number of each of the fibers. For an optical hopfion, the projected three-sphere, which we call optical hypersphere, describes the full polarization state of paraxial light, similar to the Poincaré sphere. The key difference is that the position on the hypersphere also distinguishes between different phase values even for equal polarization. The linked fibers are the set of points in space with the same polarization, not distinguished with regard to phase. Note that in our design of the skyrmionic hopfion these two quantities are related, but are not necessarily so in general. Our previous report [44] on the skyrmionic hopfion showed the basic case with skyrme number 1. However, the same method, proposed in [44] with additional details in [45], can be used to construct fields expressing higher-order hopfions:

Consider the hopf map

$$h(u, v) = (2\mathrm{Re}(u^* v), 2\mathrm{Im}(u^* v), |u|^2 - |v|^2), \tag{1}$$

with $u, v \in \mathbb{C}$ and $|u|^2 + |v|^2 = 1$. It is easy to show that the right-hand side of Eq. (1) is contained in the unit 2-sphere $\mathbb{S}^2$, i.e., the set of points of unit distance in 3D space. This map $h : \mathbb{S}^3 \to \mathbb{S}^2$ defines the mathematical hopf fibration. Through the use of stereographic projection, the total space that is the three-sphere, is mapped into real 3D space. Additional confinement by, e.g., $\tan^{-1}$ results in the confinement of the structure within a limited space and makes it applicable in light.

Now we can generalize this map by considering the map $h(u^m, v^n)$ of integer powers of u and v. The target space is guaranteed to be $\mathbb{S}^2$ if $|u^m|^2 + |v^n|^2 = 1$. But the fibration, i.e., the decomposition into preimages h^{-1}, will change depending on the indices m and n. $\mathbb{S}^3$ will be covered $m \cdot n$ times. The resulting fibers will be, once stereographically projected into real space, in the configurations of (m, n)-torus knots and links. Any two of the fibers are then linked $m \cdot n$ times, equal to the covering of $\mathbb{S}^3$. The fibers will be knotted only if the indices are co-prime. Otherwise, a fiber will be separated into d components, where d is the greatest common denominator of m and n. Therefore, the most basic knotted hopfion, meaning a hopfion where individual fibers are knots instead of an unknot, would have indices (3,2) or (2,3) with a skyrme or linking number of 6. The linking of the polarization fibers also needs some attention. It is possible to have multiple polarization fibers of the same polarization state linked with each other. For this, the simplest case is $m = n = 2$. Otherwise, for every hopfion, polarization fibers of different polarization states are always linked, the simplest case being the normal hopfion, as represented in [44]. Higher orders need increasingly complex field configurations. In the following, we will investigate the higher-order case of $m = 1$, $n = 2$ with doubly linked (but not knotted) polarization fibers as a case study of an optical higher-order skyrmionic hopfion.

Identifying u and v in Eq. (1) with a right-handed circularly polarized field E_R and a left-handed circularly polarized field E_L, respectively, immediately gives the Stokes parameters as the target space

$$h(E_\mathrm{R}, E_\mathrm{L}) = (2\mathrm{Re}(E_\mathrm{R}^* E_\mathrm{L}), \quad 2\mathrm{Im}(E_\mathrm{R}^* E_\mathrm{L}),$$
$$|E_\mathrm{R}|^2 - |E_\mathrm{L}|^2) = (s_1, s_2, s_3), \tag{2}$$

where the condition $|u|^2 + |v|^2 = |E_\mathrm{R}|^2 + |E_\mathrm{L}|^2 = 1$ normalizes the Stokes parameters (then denoted by capital S_i) and the target space is the Poincaré sphere.

Stereographically projecting E_R and E_L^2 while setting $z = 0$ will give us polynomials in r and $e^{i\varphi}$:

$$E_{\mathrm{R,2D}} = r^4 - 1,$$
$$E_{\mathrm{L,2D}} = e^{2i\varphi}. \tag{3}$$

In particular, the field will require a phase vortex on the propagation axis and a closed phase vortex loop in the focal plane. The polynomials will become physical by multiplying with a Gaussian beam. The desired light field can then be expanded in terms of Laguerre–Gaussian (LG) modes:

$$\mathrm{LG}_{l,p}(r,\varphi,z) = C_{l,p}\frac{w_0}{w(z)}\left(\frac{\sqrt{2}r}{w(z)}\right)^{|l|} L_p^{|l|}\left(\frac{2r^2}{w^2(z)}\right)\exp\left(-\frac{r^2}{w^2(z)}\right) \times \exp\left(i\left(\frac{-kr^2}{2R(z)}\right) - l\varphi + (N+1)\chi_G\right), \tag{4}$$

where l is the azimuthal mode number, p is the radial mode number, $C_{l,p}$ is a normalization factor, $w(z)$ is the beam radius with the beam waist $w_0 = w(0)$, $L_p^{|l|}$ is an associated Laguerre polynomial, k is the wavenumber, $R(z)$ is the radius of the wavefront curvature, and χ_G is the Gouy phase weighted with the combined mode number $N = 2p + |l|$. We use LG modes because they form a complete basis in the focal plane and are a natural choice for fields with phase vortices and rotational symmetry. It is important to note that the choice of embedding the polynomials in a Gaussian beam means that the results are no longer exact but in an approximation. However, the structure is still transferred. All fibers of equal ellipticity, i.e., same value for the normalized third Stokes parameter S_3, build a torus as well, but now wind twice around it in poloidal direction. Interestingly, this approach shows similarities to the method of Gao *et al.* [24]. Indeed, we expect a baby skyrmion formation in the focal plane, as every polarization state has to pass through that particular transverse plane. However, the evolution along propagation will differ.

3. RESULTS

The expansion in LG modes and introduction of optimization parameters gives a superposition of three modes for E_R and a single mode for E_L:

$$E_\mathrm{R} = (-a + 2S^4)\mathrm{LG}_{0,0} - 4S^4\mathrm{LG}_{0,1} + 2S^4\mathrm{LG}_{0,2},$$
$$E_\mathrm{L} = \mathrm{LG}_{2,0}, \tag{5}$$

where $a \geq 0$ and $S \geq 1$ are optimization parameters. The parameters are introduced in this particular way because it proved helpful in the experimental realization. The parameter S would scale the structure down in the transverse dimension, while a would control the relative intensity of E_R on the axis. However, it is also possible to use one parameter for each mode with higher p and scale it relative to the ground mode with $p = 0$, while keeping the phase relation intact. Both beams' transverse intensities and phase profiles, as well as the intensity and phase of E_R along propagation, are visualized in Fig. 1. Notably, the phase vortex loop in E_R is indicated by two oppositely charged phase vortices in the $x-z$ cut. Note that the choice of a positive charge l for the phase vortex in E_L will result in a negative skyrme number as well as linking number. In this form, a, S, the beam waist w_0 common to all LG modes, and the intensity ratios of the two beams are parameters to be set for the generation of the hopfion structure, which is especially important in the experiment. The most important indication for a successful generation was a closed left-handed C line loop around the focal plane. The measurement was made with $a = 1$, $S = 1.5$, $w_0 = 88.5$ μm, and a ratio of maximal intensities $I_{\mathrm{R,m}}/I_{\mathrm{L,m}}$ in the focal plane of approximately 6.5 in a cuboid of size of $4.15w_0 \times 4.15w_0 \times 0.69z_\mathrm{R}$, where $z_\mathrm{R} = kw_0^2/2 = 46.3$ mm is the Rayleigh length, with $k = 2\pi/\lambda$ the wavenumber and $\lambda = 532$ nm the wavelength of the light. The z range of the cuboid was scanned with 101 transverse planes.

The experimental results are obtained from the superposition of two beams. The two required beams are structured separately on a single spatial light modulator (SLM) using a split-screen approach, then set to orthogonal circular polarization and superimposed on the optical axis. The measurement of the Stokes parameters is based on the combination of a quarter-wave plate (QWP) and a horizontal polarizer in front of the camera. To be able to scan the light field along the propagation direction, the SLM and the image plane of the camera are set in a Fourier relation by an additional lens, and digital propagation is employed to identify the different planes in propagation direction. A correct reconstruction then requires to display the Fourier transform of the modes on the SLM. A detailed description of this method can be found in [44]. We extracted the

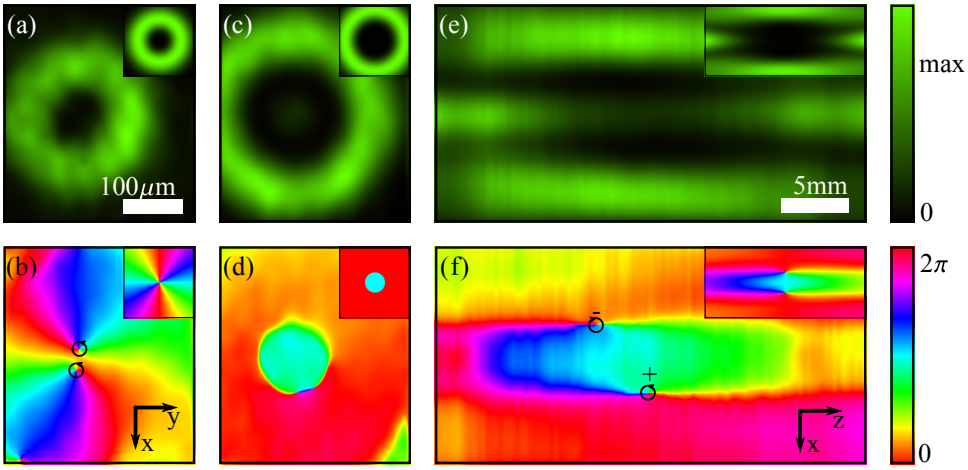

Fig. 1. Experimentally determined intensities and phases of the beams building the higher-order hopfion. Insets show the numerically determined data for comparison. (a) Intensity and (b) phase of the left-handed circularly polarized beam in the focal plane. The strength 2 phase vortex near the center (compare inset) is split into two strength 1 vortices, indicated by the circular arrows. (c), (d) Respective data for the right-handed circularly polarized beam. The phase vortex ring (visible as a phase jump in the numerics) is tilted with regard to the focal plane, and two oppositely charged phase vortices appear. (e), (f) Intensity and phase in an $x-z$ cut (z: propagation axis) along the beam center to highlight the longitudinal phase vortices, indicated by the circular arrows; + and − indicate their orientations. Note that the pictures of intensity are scaled to their respective maximum. In the focal plane, the ratio $I_{\mathrm{R,m}}/I_{\mathrm{L,m}}$ of maximal intensity is approximately 6.5. The total sizes of the measured volume are approximately 367 μm in x and y directions and 63.8 mm in z direction.

phase from a polarization measurement by superimposing one of the beams with a plane wave of orthogonal polarization. In the case of a circular polarization basis for the constituent beams, the complex Stokes field

$$\Sigma_{12} = S_1 + iS_2 = 2A_R A_L \exp\left(i\left(\chi_L - \chi_R\right)\right), \tag{6}$$

with A_j being the amplitude and χ_j being the phase of the respective right- or left-handed circularly polarized beam, will carry the same phase structure as the measured beam [46], since the plane wave introduces only a constant offset. Additionally, the intensities of the individual beams are recorded to calculate the transverse energy flow (see Section 2 in Supplement 1).

A. Polarization Structure

The experimentally determined polarization fibration is exemplified in Figs. 2(a)–2(d). Additional images with an alternative visualization are also presented in Fig. S1 in Supplement 1. The left-handed and linear polarization states close on themselves and pass twice through every other filament. This is exemplarily visualized in Fig. 2(**c**), where only three polarization fibres are drawn. All polarization filaments wind in the same manner around the left-handed C line and build tori of equal ellipticity S_3. Thus, all polarization states are linked twice. The z axis lets one define a direction of rotation of the polarization filaments around the left-handed C line. Following it in a counterclockwise direction, the polarization filaments pass through the C line loop in a counterclockwise direction also. This sense of direction is defined by the positive topological charge in E_L.

The right-handed elliptical states do not fully close on themselves, meaning that the respective S_3 surface is not closed at the z planes within the measured volume. However, the filaments generally behave according to the expectation shown in Fig. 2(e). They all pass twice through the left-handed C line and retain the correct sense of rotation around the left-handed C line, i.e., passing through the center of the C line loop in a counterclockwise fashion. Indeed, such splitting of polarization states is expected to occur above a critical value of S_3 even in the numerical simulations due to the embedding in physical beams. Because of experimental error, however, this value is drastically reduced in the experiment. Nonetheless, most of the desired topology is still expressed in the measured field.

The right-handed C line requires some additional attention. It is determined by the phase vortex in E_L. Because a vortex of charge $|l| = 2$ is required for the construction of the second-order hopfion and is unstable under perturbation [7], the phase vortex and therefore also the resulting C line are split into two singly charged lines. This results in a region between the two C lines with high value of S_3, beginning around $S_3 = 0.8$. Furthermore, it creates a strong transverse two-fold rotational symmetry of the light field.

Since phase vortices with higher topological charges are required for all higher-order hopfions—with exception for $(m, 1)$-hopfions—this limits the full embedding of these constructs. However, as shown previously, most of the structure is concentrated at lower values of S_3, which are not as much disturbed by the splitting of the C line; $(m, 1)$-hopfions do not require phase vortices with higher order, but require a superposition of multiple modes with singly charged phase vortices, which then can also split in the experiment. In turn, the left-handed C line loop has a higher charge, which will collapse under perturbation [47].

B. Skyrme Number

As discussed before, two numbers are associated with a skyrmionic hopfion: the hopf invariant or linking number and the skyrme number. For our higher-order hopfion, these values are expected

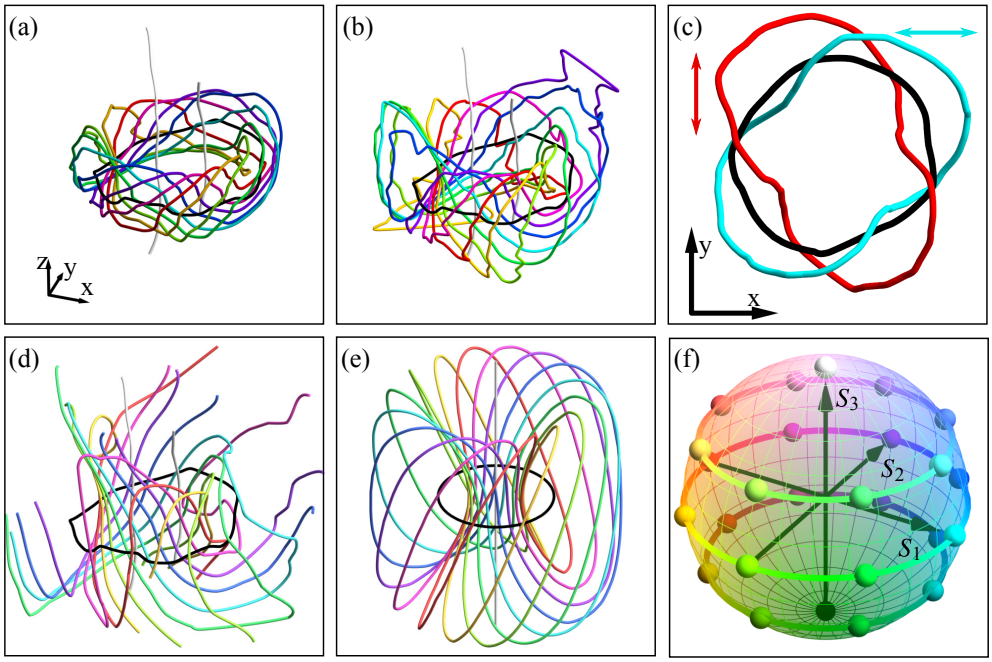

Fig. 2. Polarization fibration of the second-order hopfion at different values of S_3 in the (a)–(d) experiment and (e) simulation. The filaments are colored according to their position on the (f) Poincaré sphere, with the right- and left-handed C lines colored white and black, respectively. Note that, because the right-handed C line would have a singularity index of 2, it is split into two C-lines of singularity index 1. (a) Left-handed elliptical polarization states with $S_3 = -0.5$; (b), (c) linear polarization states with $S_3 = 0$; and right-handed elliptical polarization states with $S_3 = 0.5$ in (d) experiment and (e) simulation. (c) Vertical and horizontal polarization states as well as the left-handed C line from the top view.

to equal two. Whereas ideally both are integer valued, this is not the case due to the embedding in light fields satisfying the paraxial Helmholtz equation. However, they are still informative quantities. As seen in Fig. 2, most polarization filaments are linked twice. The skyrme density, which integrated would give the skyrme number, can be regarded as a local, continuous measure of linking of the polarization filaments, whereas the hopf invariant is a measure of the global topology.

The skyrme density Σ is related to the angles α, β, γ parametrizing the optical hypersphere [44]

$$\Sigma = \frac{1}{16\pi^2}\nabla\gamma \cdot (\nabla(\cos\beta) \times \nabla\alpha)\,, \tag{7}$$

where ∇ denotes differentiation with regard to space. As the hypersphere distinguishes polarization and phase, the angles get a physical meaning in describing a specific polarization and phase state. $-\pi < \alpha = \arctan(S_1, S_2) \leq \pi$ describes the polarization azimuth, $0 \leq \beta = \arccos(S_3) \leq \pi$ is the ellipticity, and $-2\pi < \gamma = \chi_R + \chi_L \leq 2\pi$ is the sum of the phases of the two constituent fields. In a further step, the skyrme density can also be expressed with the orbital current $\boldsymbol{J}_o = \mathrm{Im}[E_R^*\nabla E_R + E_L^*\nabla E_L] = I_R\nabla\chi_R + I_L\nabla\chi_L$, where I_j and χ_j are, respectively, the spatially varying intensity and phase of the respective beam:

$$\Sigma = \frac{1}{4\pi^2}\boldsymbol{J}_o \cdot \nabla \times \boldsymbol{J}_o. \tag{8}$$

Note that the electric fields and therefore intensities are normalized. This can be further simplified. Separating the optical current into two terms associated with the constituent beams $\boldsymbol{J}_o := \boldsymbol{J}_{o,R} + \boldsymbol{J}_{o,L}$ gives the following terms:

$$\begin{aligned}\Sigma = \frac{1}{4\pi^2}\big[&\boldsymbol{J}_{o,R} \cdot \nabla \times \boldsymbol{J}_{o,R} + \boldsymbol{J}_{o,R} \cdot \nabla \times \boldsymbol{J}_{o,L} \\ &+ \boldsymbol{J}_{o,L} \cdot \nabla \times \boldsymbol{J}_{o,R} + \boldsymbol{J}_{o,L} \cdot \nabla \times \boldsymbol{J}_{o,L}\big].\end{aligned} \tag{9}$$

The terms associated with only one beam, i.e., $\boldsymbol{J}_{o,R} \cdot \nabla \times \boldsymbol{J}_{o,R}$ and $\boldsymbol{J}_{o,L} \cdot \nabla \times \boldsymbol{J}_{o,L}$, reduce to zero while the mixed terms remain. This means that only if two orthogonally polarized beams are superimposed in a volume can a covering of the optical hypersphere be achieved. Further simplifying Eq. (9) gives a final form for the skyrme density in terms of the intensities and phases of the constituent beams:

$$\Sigma = \frac{1}{4\pi^2}\,[I_R\nabla I_L - I_L\nabla I_R] \cdot [\nabla\chi_L \times \nabla\chi_R]\,. \tag{10}$$

Equations (7) and (10) can both be used to calculate the skyrme number. Both equations contain gradients that, in case of experimental data, have to be calculated numerically and therefore introduce errors based on the chosen method. Especially around phase vortices, special care needs to be taken. Furthermore, as already discussed in the Supplement 1 of [44], this method can give values for the skyrme number larger than $m \cdot n$. However, it gives a good estimate on the skyrme number without the need of a supercomputer. Values greater than the theoretical integer value will appear only when choosing a large volume, where either the hopfion field already unwinds in propagation direction or is limited by low intensities in the transverse plane and therefore not of experimental interest. Note that although a circular polarization base was assumed in the above calculations, the skyrme density should not be dependent on this choice. This is further indicated by the orbital flow density (see Eq. S2 in Supplement 1), which is identical to the orbital current $\boldsymbol{J}_o$ apart from a scaling factor. The total orbital flow is not dependent on the choice of the polarization basis [48]—only a subdivision into partial flows is.

The calculated skyrme number for the experimental data is -1.83 compared to -1.89 for a numeric model field with the same parameters and the same volume. Compared to the theoretical value of -2, it suggests that most of the polarization states, including the varying phase, are present twice in the measured volume. On the one hand, every polarization state is weighted equally as any other, and, because the size of an S_3-torus scales with its value, left-handed elliptical states therefore have a higher absolute density. Moreover, right-handed elliptical states also contribute overall, since only a part of them is cut off and the remaining part is in the correct configuration. On the other hand, this method does not distinguish how the optical hypersphere is covered, and some polarization states are overrepresented, which is the case near the propagation axis, where the splitting of the C line introduces additional polarization states.

4. CONCLUSION AND DISCUSSION

In this work, we have overcome the challenges that hinder research on the experimental realization of higher-order skyrmionic configurations. We were able to precisely adjust the unstable higher-order singularities in the superimposed light field in such a way that the optical skyrmionic hopfion forms in a confined volume around the focal plane. We demonstrated the fibration by examples of filaments of constant polarization with varying phase along them. The filaments link twice with each other, giving rise to a skyrme number of -1.83, calculated from the experimental data, compared to the ideal value of -2.

A discussion of the structure's stability is warranted. Typically, skyrmions need non-linear terms to stabilize them [18]. These are not present in free-space optics. Therefore, there is no reason to assume that the configuration is truly stable. Indeed, the comparison between experiment and simulation shows that perturbation unwinds the structure. However, a point for topological stability can be made. Because of its particular configuration, the hopfion can unwind only from its outer layers. In particular, it unwinds by reconnecting with polarization states coming from $\pm\infty$ in propagation direction. In that regard, the core of the structure is topologically protected. New polarization states, i.e., states with high values of S_3 near the propagation axis, emerge in pairs that should not change the skyrme number, as is suggested by the similarity of the calculated numbers. States that change the skyrme number should appear only near the edges of the volume in propagation direction. A better control of the fields, especially away from the focal plane, could therefore significantly improve the structure in future steps.

Higher-order hopfions have been theoretically described for high-energy physics [49,50] and magnetism [51], but the optical analog may prove useful for the detailed study of the hopfion structure and easy access to modifications. Notably, our optical hopfion is a solution static in time, opposed to time evolving solutions in, e.g., electromagnetics [36–39]. The design of intertwined polarization and phase, as is required for the full skyrmionic hopfion, can be considered as an example of four-dimensionally structured light. This is an alternative to the approach of spatiotemporal structuring into $(3+1)$D light (see [2,52,53] and references therein). Additionally, Gao *et al.* [24] pointed out the connection between

optical skyrmions and full-Poincaré beams. A higher-dimensional, i.e., 3D, skyrmion will have the same property, meaning that there are possible field configurations that cover $\mathbb{S}^3$ but carry skyrme number 0. Furthermore, the evolution of the (baby) skyrmion at the focal plane could be interesting to study in a further step.

The properties of skyrmionic hopfions can be applied in different areas of research. Their complex 3D texture of polarization and phase, for instance, could help model field configurations in other areas of physics, where direct access to the field parameters is not easy. Karnieli *et al.* have already pointed out the connection between spin transport in magnetization textures and light in a similar case [30], even mentioning the possibility to shape optical flow. Furthermore, as recently suggested, interactions between light and atoms would enable to excite a topologically protected configuration in atomic layers [42], where different skyrme numbers could then act as units of information. Similarly, topological invariants have already been suggested for information transport and encryption [54]. Hopfions and skyrmions can also be considered for that role. It is important to note again that our hopfion is constructed using paraxial beams and therefore in an approximation. As such, it is only a first step and demonstrates potential hurdles for applications. A natural next step would be to investigate hopfion configurations in tightly focused light, which can be constructed from Zernike polynomials [45].

Funding. Deutsche Forschungsgemeinschaft (DE-486/23-1); Engineering and Physical Sciences Research Council (EP/S02297X/1); Horizon 2020 Framework Programme (ColOpt ITN 721465); Deutscher Akademischer Austauschdienst (DAAD PRIME); Stanford University (GLAM Fellowship); Leverhulme Trust (RP2013-K-009).

Acknowledgment. We are grateful to Jörg Imbrock and Eric Asché for conversations, advice, and research support. Authors D.E., R.D., E.O., and C.D. acknowledge partial support by the German Research Foundation (DFG) and EPSRC. E.O. acknowledges support from the DAAD PRIME program as well as the GLAM Fellowship, Stanford University.

Disclosures. The authors declare no conflicts of interest.

Data availability. Data underlying the results presented in this paper are not publicly available at this time but may be obtained from the authors upon reasonable request.

Supplemental document. See Supplement 1 for supporting material.

REFERENCES

1. H. Rubinsztein-Dunlop, A. Forbes, M. V. Berry, *et al.*, "Roadmap on structured light," J. Opt. **19**, 013001 (2017).
2. A. Forbes, M. de Oliveira, and M. R. Dennis, "Structured light," Nat. Photonics **15**, 253–262 (2021).
3. E. Otte, *Structured Singular Light Fields* (Springer Nature, 2020).
4. C. Rosales-Guzmán, B. Ndagano, and A. Forbes, "A review of complex vector light fields and their applications," J. Opt. **20**, 123001 (2018).
5. O. V. Angelsky, A. Y. Bekshaev, S. G. Hanson, C. Y. Zenkova, I. I. Mokhun, and Z. Jun, "Structured light: ideas and concepts," Front. Phys. **8**, 114 (2020).
6. J. Wang, F. Castellucci, and S. Franke-Arnold, "Vectorial light-matter interaction: exploring spatially structured complex light fields," AVS Quantum Sci. **2**, 031702 (2020).
7. E. Otte and C. Denz, "Customization and analysis of structured singular light fields," J. Opt. **23**, 73501 (2021).
8. G. J. Gbur, *Singular Optics* (CRC Press, 2017).
9. M. R. Dennis, K. O'Holleran, and M. J. Padgett, "Singular optics: optical vortices and polarization singularities," in *Progress in Optics* (Elsevier, 2009), Vol. **53**, pp. 293–363.
10. M. Soskin and M. Vasnetsov, "Singular optics," Prog. Opt. **42**, 219–276 (2001).
11. J. Wang, J. Liu, S. Li, Y. Zhao, J. Du, and L. Zhu, "Orbital angular momentum and beyond in free-space optical communications," Nanophotonics **11**, 645–680 (2022).
12. M. R. Dennis, R. P. King, B. Jack, K. O'Holleran, and M. J. Padgett, "Isolated optical vortex knots," Nat. Phys. **6**, 118–121 (2010).
13. M. J. Padgett, K. O'Holleran, R. P. King, and M. R. Dennis, "Knotted and tangled threads of darkness in light beams," Contemp. Phys. **52**, 265–279 (2011).
14. H. Larocque, D. Sugic, D. Mortimer, A. J. Taylor, R. Fickler, R. W. Boyd, M. R. Dennis, and E. Karimi, "Reconstructing the topology of optical polarization knots," Nat. Phys. **14**, 1079–1082 (2018).
15. J. A. Rodrigo, T. Alieva, E. Abramochkin, and I. Castro, "Shaping of light beams along curves in three dimensions," Opt. Express **21**, 20544–20555 (2013).
16. T. H. R. Skyrme, "A non-linear field theory," Proc. R. Soc. London A **260**, 127–138 (1961).
17. T. H. R. Skyrme, "A unified field theory of mesons and baryons," Nucl. Phys. **31**, 556–569 (1962).
18. N. Manton and P. Sutcliffe, *Topological Solitons* (Cambridge University, 2004).
19. N. Nagaosa and Y. Tokura, "Topological properties and dynamics of magnetic skyrmions," Nat. Nanotechnol. **8**, 899–911 (2013).
20. W. Kang, Y. Huang, C. Zheng, W. Lv, N. Lei, Y. Zhang, X. Zhang, Y. Zhou, and W. Zhao, "Voltage controlled magnetic skyrmion motion for racetrack memory," Sci. Rep. **6**, 23164 (2016).
21. S. Donati, L. Dominici, G. Dagvadorj, D. Ballarini, M. De Giorgi, A. Bramati, G. Gigli, Y. G. Rubo, M. H. Szymańska, and D. Sanvitto, "Twist of generalized skyrmions and spin vortices in a polariton superfluid," Proc. Natl. Acad. Sci. USA **113**, 14926–14931 (2016).
22. S. Tsesses, E. Ostrovsky, K. Cohen, B. Gjonaj, N. H. Lindner, and G. Bartal, "Optical skyrmion lattice in evanescent electromagnetic fields," Science **361**, 993–996 (2018).
23. L. Du, A. Yang, A. V. Zayats, and X. Yuan, "Deep-subwavelength features of photonic skyrmions in a confined electromagnetic field with orbital angular momentum," Nat. Phys. **15**, 650–654 (2019).
24. S. Gao, F. C. Speirits, F. Castellucci, S. Franke-Arnold, S. M. Barnett, and J. B. Götte, "Paraxial skyrmionic beams," Phys. Rev. A **102**, 053513 (2020).
25. Y. Shen, E. C. Martínez, and C. Rosales-Guzmán, "Generation of optical skyrmions with tunable topological textures," ACS Photon. **9**, 296–303 (2022).
26. A. O. Leonov and M. Mostovoy, "Multiply periodic states and isolated skyrmions in an anisotropic frustrated magnet," Nat. Commun. **6**, 8275 (2015).
27. L. Rózsa, K. Palotás, A. Deák, E. Simon, R. Yanes, L. Udvardi, L. Szunyogh, and U. Nowak, "Formation and stability of metastable skyrmionic spin structures with various topologies in an ultrathin film," Phys. Rev. B **95**, 094423 (2017).
28. D. Foster, C. Kind, P. J. Ackerman, J.-S. B. Tai, M. R. Dennis, and I. I. Smalyukh, "Two-dimensional skyrmion bags in liquid crystals and ferromagnets," Nat. Phys. **15**, 655–659 (2019).
29. B. Göbel, I. Mertig, and O. A. Tretiakov, "Beyond skyrmions: review and perspectives of alternative magnetic quasiparticles," Phys. Rep. **895**, 1–28 (2021).
30. A. Karnielie, S. Tsesses, G. Bartal, and A. Arie, "Emulating spin transport with nonlinear optics, from high-order skyrmions to the topological Hall effect," Nat. Commun. **12**, 1092 (2021).
31. L. Faddeev and A. Niemi, "Stable knot-like structures in classical field theory," Nature **387**, 58–61 (1997).
32. R. A. Battye and P. M. Sutcliffe, "Knots as stable soliton solutions in a three-dimensional classical field theory," Phys. Rev. Lett. **81**, 4798–4801 (1998).
33. J. Hietarinta and P. Salo, "Faddeev-Hopf knots: dynamics of linked unknots," Phys. Lett. B **451**, 60–67 (1999).
34. A. F. Ranada, "A topological theory of the electromagnetic field," Lett. Math. Phys. **18**, 97–106 (1989).
35. A. F. Ranada, "Topological electromagnetism," J. Phys. A **25**, 1621–1641 (1992).
36. W. T. Irvine and D. Bouwmeester, "Linked and knotted beams of light," Nat. Phys. **4**, 716–720 (2008).
37. H. Kedia, I. Bialynicki-Birula, D. Peralta-Salas, and W. T. Irvine, "Tying knots in light fields," Phys. Rev. Lett. **111**, 150404 (2013).

38. W. Lee, A. H. Gheorghe, K. Tiurev, T. Ollikainen, M. Möttönen, and D. S. Hall, "Synthetic electromagnetic knot in a three-dimensional skyrmion," Sci. Adv. **4**, eaao3820 (2018).
39. A. Thompson, A. Wickes, J. Swearngin, and D. Bouwmeester, "Classification of electromagnetic and gravitational hopfions by algebraic type," J. Phys. A **48**, 205202 (2015).
40. P. J. Ackerman, J. Van De Lagemaat, and I. I. Smalyukh, "Self-assembly and electrostriction of arrays and chains of hopfion particles in chiral liquid crystals," Nat. Commun. **6**, 6012 (2015).
41. P. J. Ackerman and I. I. Smalyukh, "Static three-dimensional topological solitons in fluid chiral ferromagnets and colloids," Nat. Mater. **16**, 426–433 (2017).
42. C. D. Parmee, M. R. Dennis, and J. Ruostekoski, "Optical excitations of skyrmions, knotted solitons, and defects in atoms," Commun. Phys. **5**, 54 (2022).
43. Y. Shen, B. Yu, H. Wu, C. Li, Z. Zhu, and A. V. Zayats, "Topological transformation and free-space transport of photonic hopfions," Adv. Photon. **5**, 015001 (2023).
44. D. Sugic, R. Droop, E. Otte, D. Ehrmanntraut, F. Nori, J. Ruostekoski, C. Denz, and M. R. Dennis, "Particle-like topologies in light," Nat. Commun. **12**, 6785 (2021).
45. D. Sugic, "Unravelling the dark focus of light: a study of knotted optical singularities," Ph.D. thesis (University of Bristol, 2019).
46. I. Freund, "Poincaré vortices," Opt. Lett. **26**, 1996–1998 (2001).
47. M. V. Berry and M. R. Dennis, "Knotted and linked phase singularities in monochromatic waves," Proc. R. Soc. A **457**, 2251–2263 (2001).
48. A. Y. Bekshaev and M. S. Soskin, "Transverse energy flows in vectorial fields of paraxial beams with singularities," Opt. Commun. **271**, 332–348 (2007).
49. M. Kobayashi and M. Nitta, "Toroidal domain walls as hopfions," arXiv, arXiv:1304.4737 (2013).
50. M. Kobayashi and M. Nitta, "Torus knots as hopfions," Phys. Lett. B **728**, 314–318 (2014).
51. N. Kent, N. Reynolds, D. Raftrey, I. T. Campbell, S. Virasawmy, S. Dhuey, R. V. Chopdekar, A. Hierro-Rodriguez, A. Sorrentino, E. Pereiro, and S. Ferrer, "Creation and observation of hopfions in magnetic multilayer systems," Nat. Commun. **12**, 1562 (2021).
52. K. Y. Bliokh and F. Nori, "Spatiotemporal vortex beams and angular momentum," Phys. Rev. A **86**, 033824 (2012).
53. A. Chong, C. Wan, J. Chen, and Q. Zhan, "Generation of spatiotemporal optical vortices with controllable transverse orbital angular momentum," Nat. Photonics **14**, 350–354 (2020).
54. H. Larocque, A. D'Errico, M. F. Ferrerer-Garcia, A. Carmi, E. Cohen, and E. Karimi, "Optical framed knots as information carriers," Nat. Commun. **11**, 5119 (2020).